Functionalized NbS_2 as cathode for Li- and Na-ion batteries

Jiajie Zhu, Husam N. Alshareef, and Udo Schwingenschlögl

Citation: Appl. Phys. Lett. **111**, 043903 (2017); doi: 10.1063/1.4985694
View online: http://dx.doi.org/10.1063/1.4985694
View Table of Contents: http://aip.scitation.org/toc/apl/111/4
Published by the American Institute of Physics

Functionalized NbS_2 as cathode for Li- and Na-ion batteries

Jiajie Zhu,[1,2] Husam N. Alshareef,[2] and Udo Schwingenschlögl[2,a)]
[1]College of Materials Science and Engineering, Shenzhen University, Nanhai Ave 3688, ShenZhen, Guangdong 518060, People's Republic of China
[2]King Abdullah University of Science and Technology (KAUST), Physical Science and Engineering Division (PSE), Thuwal 23955-6900, Saudi Arabia

(Received 1 June 2017; accepted 18 July 2017; published online 27 July 2017)

Cathodes of Li- and Na-ion batteries usually have capacities <200 mAh/g, significantly less than the anodes. Two-dimensional materials can overcome this limitation but suffer from low voltages. In this context, we investigate NbS_2 functionalized by O, F, and Cl as a cathode material by first-principles calculations, considering both the conversion and intercalation mechanisms. NbS_2O_2 shows a higher voltage than NbS_2 for both Li and Na, but the voltage decreases drastically for increasing ion coverage. Even higher voltages and favorable dependences on the ion coverage are achieved by F and Cl functionalization. We obtain NbS_2F_2 and NbS_2Cl_2 energy densities of 1223 mW h/g and 823 mW h/g for lithiation and 1086 mW h/g and 835 mW h/g for sodiation, respectively. These values are higher than those for most state-of-the-art cathode materials (~600 mW h/g). In addition, low diffusion barriers enable high cycling rates. *Published by AIP Publishing.*
[http://dx.doi.org/10.1063/1.4985694]

Nowadays, batteries, fuel cells, and supercapacitors are attracting much attention as energy storage and conversion devices, motivated by a rapidly increasing global energy consumption. Rechargeable Li-ion batteries, using Li ions for the charge transfer, are replacing lead-acid, Ni-Cd, and nickel-metal-hydride batteries because of environmental concerns due to the toxic metals. A high energy density, the absence of memory effects, and a long cycle life enable Li-ion batteries to be widely used in portable electronic devices such as cell phones, laptops, and cameras.[1,2] However, scarcity and associated high costs of Li limit its field of applications. Na-ion batteries have been considered as promising alternatives in large scale devices, such as electric vehicles and power grids, since their properties are similar and Na has the advantage of natural abundance.[3]

The anode and cathode materials used in commercial Li-ion batteries are graphite and transition metal oxides, respectively, with the operation being based on the intercalation mechanism.[4] Since graphite has a low theoretical capacity of 372 mA h/g,[5] various alternatives with capacities >600 mA h/g have been proposed, including SnO_2,[6] graphene,[7] and silicene.[8] Phosphorene has been put forward as a high capacity anode material for Na-ion batteries.[9,10] The operational voltages of most cathode materials for Li-ion batteries range from 3 V to 4 V with an energy density (product of voltage and capacity) of some 600 mW h/g, rarely reaching 900 mW h/g.[11] Similar limitations of the energy density apply to Na-ion batteries.[12] Since the typical cathode capacity is <200 mA h/g, i.e., significantly lower than that of the anode, and the voltage is bound by the stability limit of the electrolyte (usually 4.6 V),[11,12] it is effective to improve the energy density by enhancing the capacity.

Two-dimensional materials have been predicted to provide high Li and Na capacities as anodes due to their large surface areas.[13,14] In addition, low diffusion barriers (flat potential surfaces) enable high cycling rates.[15,16] However, weak interactions with ions lead to low and decreasing voltages in the intercalation reactions, which limits their application as cathodes.[17,18] Electrodes employing conversion mechanisms usually yield higher voltages.[4] On the other hand, it is known from MXenes that functionalization can be used to tailor the surface properties of two-dimensional materials, in particular the interaction with ions.[19,20] Monolayer transition metal dichalcogenides, which can be exfoliated from bulk crystals,[21] are semiconducting when they are based on Mo and W, whereas NbS_2 is a metallic member of the family and therefore interesting from the battery point of view. Indeed, bulk NbS_2 has been considered as an anode in Na-ion batteries, providing a voltage below 1 V.[22] We study in the present work the potential of monolayer NbS_2 functionalized by O, F, and Cl (chosen because of the high electronegativities[23]) as a cathode material for Li- and Na-ion batteries, considering both the conversion and intercalation mechanisms.

Lithiation and sodiation of monolayer NbS_2 are investigated using 2×2 in-plane supercells with a vacuum layer of 15 Å thickness in the out-of-plane direction to enable the application of three-dimensional periodic boundary conditions. Total energy calculations are carried out in the framework of the density functional theory and the projector augmented wave method, as implemented in the Vienna *Ab-initio* Simulation Package.[24] The exchange correlation potential is modeled in the generalized gradient approximation of Perdew, Burke, and Ernzerhof.[25] In addition, the long-range van der Waals interaction is taken into account by means of the DFT-D3 approach.[26] The cut-off energy of the plane wave basis is set to 500 eV and the energy criterion of the iterative solution of the Kohn-Sham equations to 10^{-6} eV. All structures are relaxed until the residual forces on the atoms have declined to less than 0.01 eV/Å. Brillouin zone integrations are performed on a $6 \times 6 \times 1$ k-mesh. All the technical parameters have been tested carefully for convergence. The nudged elastic band method[27] with 9 images

a)Email: udo.schwingenschlogl@kaust.edu.sa

between the initial and final states is employed to evaluate the diffusion paths and barriers.

The in-plane lattice constant of H-phase[16] NbS_2 is calculated to be 3.33 Å, in good agreement with the experimental value of 3.31 Å.[22] O, F, and Cl functionalization modifies it to 3.28 Å, 3.45 Å, and 3.48 Å, being stable with negative formation energies of –0.86 eV, –1.39 eV, and –0.03 eV, respectively. We note that these values are modified by less than 0.01 eV when the vdWB86b functional is used instead of the DFT-D3 approach. Formation energies, ΔH, here and in the following are defined as differences between the total energy of a combined system and the sum of the total energies of its parts. Since the absolute value is very small for Cl functionalization, we have confirmed the stability by *ab-initio* molecular dynamics simulations for 4 ps at 300 K. This result is also supported by the fact that NbS_2Cl_2 has been prepared experimentally in Ref. 28. In addition, *ab-initio* molecular dynamics simulations exclude the reaction of Li/Na with NbS_2 and structural collapse during lithiation and sodiation. Comparison to the T-phase[16] shows for all functionalizations and coverages considered in this study that the H-phase is favorable. The S-O (1.48 Å), S-F (1.69 Å), and S-Cl (2.13 Å) bond lengths are influenced by both the charge transfer and the ionic radius.

Figure 1 shows the structures of NbS_2O_2 decorated with Li/Na on top of the (a) Nb and (b) hollow sites. These two configurations turn out to be energetically almost degenerate for low Li/Na coverage, while decoration on top of the O/F/Cl site results in significantly higher total energy. For high Li/Na coverage, on the other hand, decoration on top of the Nb site is found to be favorable. We note that decoration on top of the bridge site always results in relaxation toward configuration (a). The perpendicular distance between Li/Na and O relaxes to 0.75/1.11 Å, mostly determined by the ionic radius of Li/Na, and negative formation energy associated with the decoration (–4.23/–3.95 eV) reflects stability. For bare NbS_2, this formation energy amounts to –2.03/–1.80 eV. Since the Coulomb interaction determines the stability, we summarize the charge transfers obtained from Bader atomic charges in Table I. Mainly, S and O are affected by charge transfer due to the presence of Li/Na. This effect is also

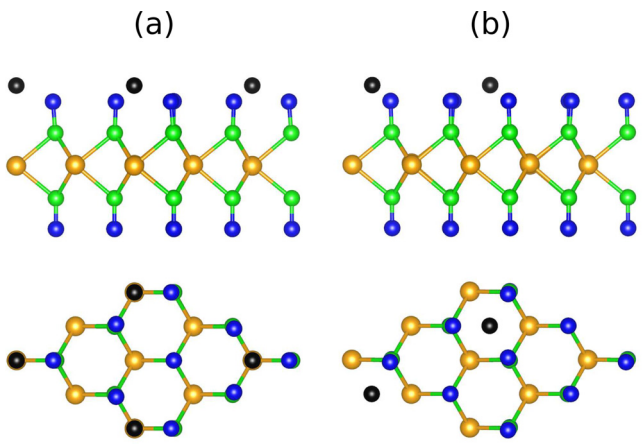

FIG. 1. Side and top views of NbS_2O_2 decorated with Li/Na on top of the (a) Nb and (b) hollow sites. Nb, S, O, and Li/Na atoms are shown in light brown, green, blue, and black color, respectively.

TABLE I. Charge transfers affecting Nb, S, O, and Li/Na in NbS_2:Li/Na and NbS_2O_2:Li/Na (obtained from Bader charges). Positive and negative values represent the charge depletion and accumulation, respectively.

	Nb	S	O	Li/Na
NbS_2	+1.58	−0.79	…	…
NbS_2:Li	+1.51	−0.98	…	+0.86
NbS_2:Na	+1.55	−0.96	…	+0.82
NbS_2O_2	+1.22	+0.35	−0.96	…
NbS_2O_2:Li	+1.24	+0.20	−1.09	+0.88
NbS_2O_2:Na	+1.24	+0.18	−1.04	+0.86

visible in Fig. 2 just above the Fermi energy by a reduction in the S 3*p* and O 2*p* densities of states. Both before and after Li/Na decoration, the system is metallic, with Nb 4*d* (dominating), S 3*p*, and O 2*p* contributions at the Fermi energy.

In order to evaluate whether NbS_2O_2 can provide the high voltage required by a cathode material, the voltage[29]

$$V = \frac{E[x_2] - E[x_1] - (x_2 - x_1) \cdot E[\mathrm{Li/Na}]}{x_2 - x_1}, \tag{1}$$

with respect to bulk Li/Na (where E is the total energy and x the Li/Na coverage) is addressed in Fig. 3 for different reaction mechanisms. The conversion reaction

$$NbS_2O_2 + 2z \cdot Li = NbS_2O_{2-z} + z \cdot Li_2O, \tag{2}$$

yields almost flat voltages of 2.8 V and 1.9 V for lithiation and sodiation, respectively. The voltages obtained for the intercalation reaction

$$NbS_2O_2 + z \cdot Li = NbS_2O_2Li_z, \tag{3}$$

initially are much higher, 4.2 V and 3.9 V, but decrease fast due to the repulsion between the Li/Na ions, reaching values of 1.8 V and 1.1 V at a coverage of 2 ions per NbS_2O_2 unit

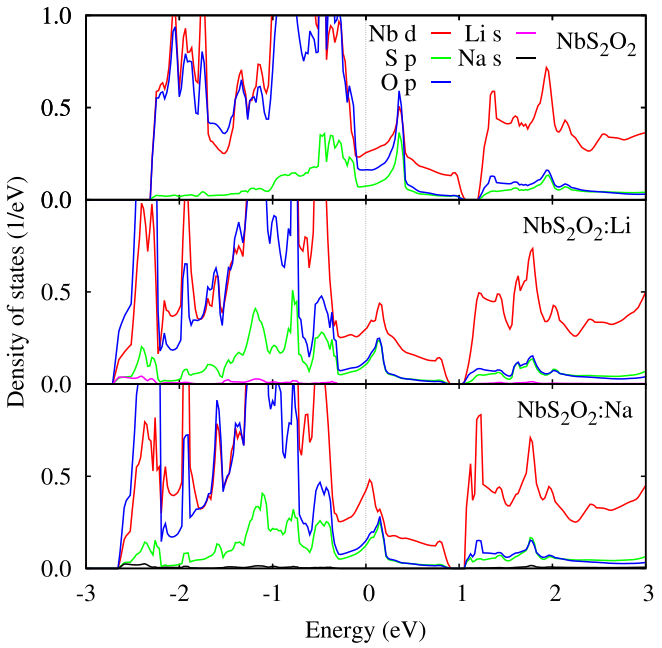

FIG. 2. Partial densities of states of NbS_2O_2 and NbS_2O_2:Li/Na. The energy zero is the Fermi energy.

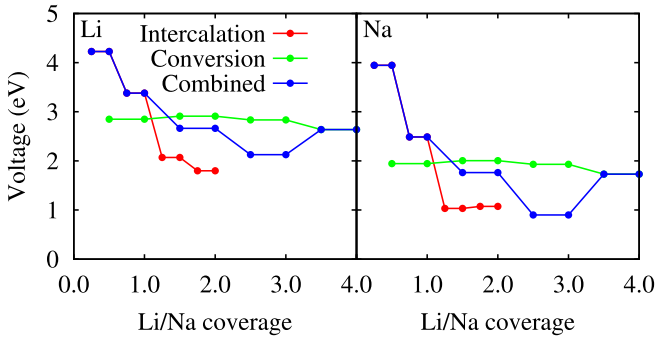

FIG. 3. Voltage for NbS_2O_2 as a function of the Li/Na coverage.

cell. Turning to the combination of the two mechanisms, we assume that Li/Na is located near O, as we have shown before that the formation energy is much less negative for NbS_2 than for NbS_2O_2. When the coverage is not more than 1, then the removal of intercalated Li/Na and O is endothermic, reflecting stability, while conversion becomes exothermic for higher coverage. However, the voltage obtained for the combined reactions is lower than that obtained for pure conversion, see Fig. 3, because O needs to overcome the interaction with other ions. The required value of about 3 V is achieved only for low coverage.

In order to improve the voltage, we replace different amounts of O with F or Cl. F has a higher electronegativity than O, and Cl can be easily removed from NbS_2 (formation energy close to zero, see above). Figure 4 shows the voltages for $NbS_2(O_{1-x}F_x)_2$ and $NbS_2(O_{1-x}Cl_x)_2$ for $0 \leq x \leq 1$. Conversion of F is always more exothermic than intercalation, which leads to the complete removal of F before intercalation begins. A similar behavior is found for Cl, except for $x = 0.25$ where Cl is converted after two Li/Na ions have been intercalated near O atoms. The lithiation and sodiation voltages of NbS_2F_2 range from 4.4 V to 5.2 V and from 3.9 V to 4.7 V, respectively, being higher than in the case of NbS_2Cl_2 (from 3.5 V to 4.3 V) due to more negative cohesive energies of LiF/NaF (−4.56/−4.08 eV) as compared to those of LiCl/NaCl (−3.55/–3.34 eV). As compared to NbS_2O_2, the voltages are much higher, while the maximal coverage is much smaller. In addition, the lowest observed voltages increase with x for both F and Cl, see Fig. 4. After F/Cl is completely converted, the voltages equal those of NbS_2O_2. We note that the generalized gradient approximation[25] usually underestimates the calculated voltages.[30] Improved descriptions of the exchange correlation potential would predict even better battery performance for functionalized NbS_2.[31,32]

Figure 5 shows for $NbS_2(O_{1-x}F_x)_2$ and $NbS_2(O_{1-x}Cl_x)_2$ for $0 \leq x \leq 1$ the energy density calculated as a product of the lowest voltage that still exceeds the 3 V threshold and the capacity, $C = x \cdot F/M$, where F is the Faraday constant and M is the atomic mass.[29] The obtained capacities exceed that of the commercial cathode $LiCoO_2$, for example, Ref. 11. The energy densities increase significantly with x, exceeding for lithiation and sodiation the ∼600 mW h/g threshold of most state-of-the-art cathode materials for $x > 0.25$ and 0.50, respectively. Energy densities of 1223 mW h/g (F functionalization) and 823 mW h/g (Cl functionalization) can be achieved for lithiation, while for sodiation, the corresponding values are 1086 mW h/g and 835 mW h/g. According to Ref. 28, NbS_2Cl_2 cathodes for Na-ion batteries provide an open circuit voltage of 3.2 V, a capacity of 120 mA h/g, and an energy density of 320 mW h/g. Deviations of the capacity and energy density from the theoretical values are due to the lower experimental voltage of 3.6 V. Since NbS_2Cl_2 exists, NbS_2 in principle can be functionalized by O and F due to higher electronegativities as compared to Cl.

The diffusion paths and barriers are shown in Fig. 6, as they determine the cycling performance. We compare two diffusion paths connecting Li/Na on top of a Nb site (ground

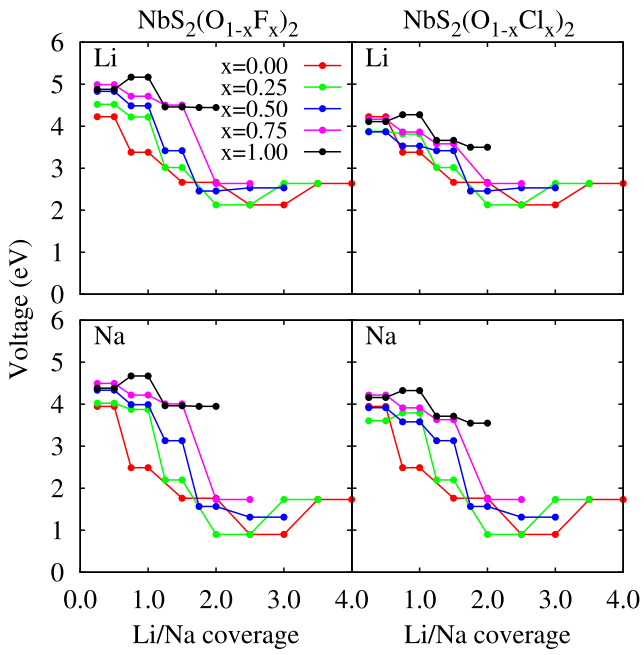

FIG. 4. Voltages for $NbS_2(O_{1-x}F_x)_2$ and $NbS_2(O_{1-x}Cl_x)_2$ as functions of the Li/Na coverage.

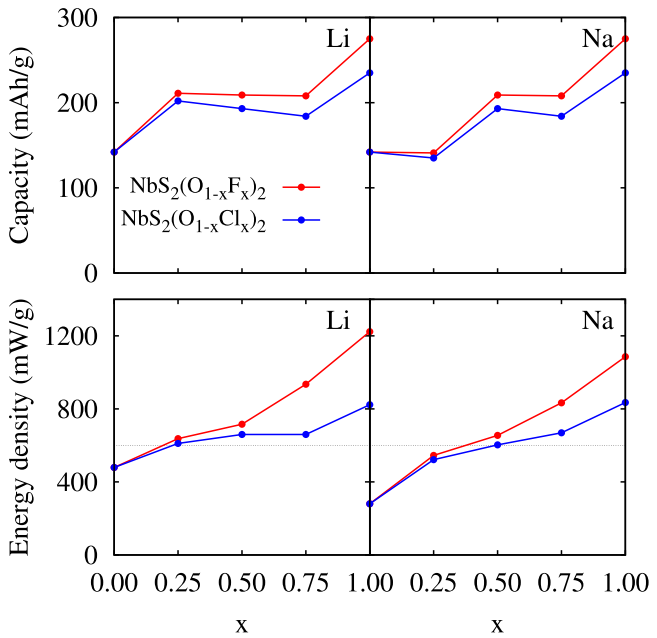

FIG. 5. Capacities and energy densities for $NbS_2(O_{1-x}F_x)_2$ and $NbS_2(O_{1-x}Cl_x)_2$ in the cases of lithiation and sodiation. The dashed line represents the typical energy density of state-of-the-art cathode materials.

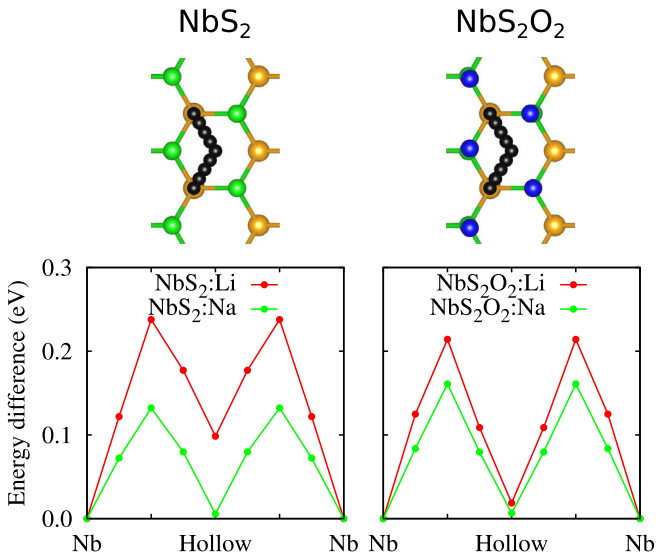

FIG. 6. Diffusion paths and barriers for NbS_2 and NbS_2O_2. The Nb, S, O, and Li/Na atoms are shown in light brown, green, blue, and black color.

state) with the nearest equivalent site for both NbS_2 and NbS_2O_2. Path A passes through the top of the hollow site, while path B is a straight connection. It turns out that path B always converges to path A. On NbS_2, we obtain diffusion barriers of 0.24 eV and 0.13 eV (in agreement with the theoretical value of Ref. 22) for Li and Na, respectively. The corresponding values on NbS_2O_2 are 0.21 eV and 0.16 eV. The interaction of Na with O increases the diffusion barrier as compared to bare NbS_2, while for Li, this effect is overcompensated by an enhanced height of the diffusion path after O functionalization. We note that the transition points are located at about one and three quarters of the diffusion path. The calculated Li diffusion barriers are comparable with the low values of other two-dimensional materials, including silicene [0.23 eV (Ref. 8)] and MoS_2 [0.21 eV (Ref. 16)].

NbS_2 functionalized by O, F, and Cl has been investigated by first-principles calculations as a potential cathode material for Li- and Na-ion batteries, considering both the conversion and intercalation mechanisms. Intercalated Li/Na ions turn out to be more strongly bound on NbS_2O_2 than NbS_2, which leads to a higher open circuit voltage. However, the voltage provided by NbS_2O_2 decreases drastically with the Li/Na coverage due to repulsion between the intercalated ions. The replacement of O with F or Cl improves the voltage due to modified conversion reactions, and this effect is found to be enhanced for increasing Li/Na coverage. In addition, F and Cl are predicted to provide almost constant voltages for low coverage. Lithiation and sodiation energy densities of 1223 mW h/g and 1086 mW h/g are obtained for NbS_2F_2 and 823 mW h/g and 835 mW h/g for NbS_2Cl_2, respectively, outperforming most current cathode materials. The diffusion barriers are found to be favorably low to enable high cycling rates. In contrast to Cl functionalization, F functionalization in the case of lithiation can result in voltages beyond the current electrolyte safety limit (4.6 V), calling for the design of alternative electrolytes. In summary, our study demonstrates how the applicability of transition metal dichalcogenides in Li- and Na-ion batteries can be extended to cathodes. The observed enhancement of the energy density opens urgently needed avenues for improving the battery performance.

The research reported in this publication was supported by funding from King Abdullah University of Science and Technology (KAUST).

[1]Y. Jing, Z. Zhou, C. R. Cabrera, and Z. Chen, "Graphene, inorganic graphene analogs and their composites for lithium ion batteries," J. Mater. Chem. A **2**, 12104–12122 (2014).
[2]W. Sun and Y. Wang, "Graphene-based nanocomposite anodes for lithium-ion batteries," Nanoscale **6**, 11528–11552 (2014).
[3]H. Kang, Y. Liu, K. Cao, Y. Zhao, L. Jiao, Y. Wang, and H. Yuan, "Update on anode materials for Na-ion batteries," J. Mater. Chem. A **3**, 17899–17913 (2015).
[4]M. V. Reddy, G. V. S. Rao, and B. V. R. Chowdari, "Metal oxides and oxysalts as anode materials for Li ion batteries," Chem. Rev. **113**, 5364–5457 (2013).
[5]K. Fukuda, K. Kikuya, K. Isono, and M. Yoshio, "Foliated natural graphite as the anode material for rechargeable lithium-ion cells," J. Power Sources **69**, 165–168 (1997).
[6]J. Zhang, L. Chang, F. Wang, D. Xie, Q. Su, and G. Du, "Ultrafine SnO_2 nanocrystals anchored graphene composites as anode material for lithium-ion batteries," Mater. Res. Bull. **68**, 120–125 (2015).
[7]Z.-S. Wu, W. Ren, L. Wen, L. Gao, J. Zhao, Z. Chen, G. Zhou, F. Li, and H.-M. Cheng, "Graphene anchored with Co_3O_4 nanoparticles as anode of lithium ion batteries with enhanced reversible capacity and cyclic performance," ACS Nano **4**, 3187–3194 (2010).
[8]G. A. Tritsaris, E. Kaxiras, S. Meng, and E. Wang, "Adsorption and diffusion of lithium on layered silicon for Li-ion storage," Nano Lett. **13**, 2258–2263 (2013).
[9]J. Qian, X. Wu, Y. Cao, X. Ai, and H. Yang, "High capacity and rate capability of amorphous phosphorus for sodium ion batteries," Angew. Chem. Int. Ed. **52**, 4633–4636 (2013).
[10]J. Sun, H.-W. Lee, M. Pasta, H. Yuan, G. Zheng, Y. Sun, Y. Li, and Y. Cui, "A phosphorene-graphene hybrid material as a high-capacity anode for sodium-ion batteries," Nat. Nanotechnol. **10**, 980–985 (2015).
[11]B. Xu, D. Qian, Z. Wang, and Y. S. Meng, "Recent progress in cathode materials research for advanced lithium ion batteries," Mater. Sci. Eng., R **73**, 51–65 (2012).
[12]X. Xiang, K. Zhang, and J. Chen, "Recent advances and prospects of cathode materials for sodium-ion batteries," Adv. Mater. **27**, 5343–5364 (2015).
[13]X. Tan, C. R. Cabrera, and Z. Chen, "Metallic BSi_3 silicene: A promising high capacity anode material for lithium-ion batteries," J. Phys. Chem. C **118**, 25836–25843 (2014).
[14]V. V. Kulish, O. I. Malyi, C. Persson, and P. Wu, "Phosphorene as an anode material for Na-Ion batteries: A first-principles study," Phys. Chem. Chem. Phys. **17**, 13921–13928 (2015).
[15]B. Ahmed, D. H. Anjum, M. N. Hedhili, and H. N. Alshareef, "Mechanistic insight into the stability of HfO_2-coated MoS_2 nanosheet anodes for sodium ion batteries," Small **11**, 4341–4350 (2015).
[16]H. Shu, F. Li, C. Hu, P. Liang, D. Cao, and X. Chen, "The capacity fading mechanism and improvement of cycling stability in MoS_2-based anode materials for lithium-ion batteries," Nanoscale **8**, 2918–2926 (2016).
[17]S. Cahangirov, M. Topsakal, E. Aktürk, H. Şahin, and S. Ciraci, "Two- and one-dimensional honeycomb structures of silicon and germanium," Phys. Rev. Lett. **102**, 236804 (2009).
[18]Y. Liao, K.-S. Park, P. Xiao, G. Henkelman, W. Li, and J. B. Goodenough, "Sodium intercalation behavior of layered Na_xNbS_2 ($0 \leq x \leq 1$)," Chem. Mater. **25**, 1699–1705 (2013).
[19]D. Er, J. Li, M. Naguib, Y. Gogotsi, and V. B. Shenoy, "Ti_3C_2 MXene as a high capacity electrode material for metal (Li, Na, K, Ca) ion batteries," ACS Appl. Mater. Interfaces **6**, 11173–11179 (2014).
[20]Y. Xie, Y. DallAgnese, M. Naguib, Y. Gogotsi, M. W. Barsoum, H. L. Zhuang, and P. R. C. Kent, "Prediction and characterization of MXene nanosheet anodes for non-lithium-ion batteries," ACS Nano **8**, 9606–9615 (2014).
[21]R. Lv, J. A. Robinson, R. E. Schaak, D. Sun, Y. Sun, T. E. Mallouk, and M. Terrones, "Transition metal dichalcogenides and beyond: Synthesis, properties, and applications of single- and few-layer nanosheets," Acc. Chem. Res. **48**, 56–64 (2015).

[22]E. Yang, H. Ji, and Y. Jung, "Two-dimensional transition metal dichalcogenide monolayers as promising sodium ion battery anodes," J. Phys. Chem. C **119**, 26374–26380 (2015).
[23]A. K. De, *A Textbook of Inorganic Chemistry* (New Age International, 2003), p 155.
[24]G. Kresse and D. Joubert, "From ultrasoft pseudopotentials to the projector augmented-wave method," Phys. Rev. B **59**, 1758–1775 (1999).
[25]J. P. Perdew, K. Burke, and M. Ernzerhof, "Generalized gradient approximation made simple," Phys. Rev. Lett. **77**, 3865–3868 (1996).
[26]S. Grimme, J. Antony, S. Ehrlich, and H. A. Krieg, "Consistent and accurate ab initio parametrization of density functional dispersion correction (DFT-D) for the 94 elements H-Pu," J. Chem. Phys. **132**, 154104 (2010).
[27]G. Mills, H. Jónsson, and G. K. Schenter, "Reversible work transition state theory: Application to dissociative adsorption of hydrogen," Surf. Sci. **324**, 305–337 (1995).
[28]K. Abraham, M. Rupich, and J. Elliot, "Rechargeable sodium batteries–VI. Cycling behavior of VS_2, '$VCl_3 + nS$' and NbS_2Cl_2 cathodes in molten $NaAlCl_4$," Electrochim. Acta **30**, 1635–1643 (1985).
[29]R. V. Kumar and T. Sarakonsri, *High Energy Density Lithium Batteries* (Wiley-VCH, 2010), pp. 1–25.
[30]F. Zhou, M. Cococcioni, C. A. Marianetti, D. Morgan, and G. Ceder, "First-principles prediction of redox potentials in transition-metal compounds with LDA+U," Phys. Rev. B **70**, 235121 (2004).
[31]J. Sun, A. Ruzsinszky, and J. P. Perdew, "Strongly constrained and appropriately normed semilocal density functional," Phys. Rev. Lett. **115**, 036402 (2015).
[32]I. G. Buda, C. Lane, B. Barbiellini, A. Ruzsinszky, J. Sun, and A. Bansil, "Characterization of thin film materials using SCAN Meta-GGA, an accurate nonempirical density functional," Sci. Rep. **7**, 44766 (2017).